Pergamon

PII: S0191-8141(96)00111-3

Journal of Structural Geology, Vol. 19, Nos 3–4, pp. 583 to 602, 1997

0191-8141/97 $17.00 + 0.00

Fault-related folding in sandbox analogue models of thrust wedges

F. STORTI and F. SALVINI

Dipartimento di Scienze Geologiche, Università degli Studi 'Roma Tre', Via Ostiense 169, 00154 Roma, Italy

and

K. McCLAY

Fault Dynamics Project, Royal Holloway, University of London, Egham, Surrey TW20 OEX, U.K.

(*Received* 9 *February* 1996; *accepted in revised form* 13 *November* 1996)

Abstract—The nucleation and growth of thrust fault-related folds has been simulated using high-resolution sandbox Coulomb wedge-type analogue models. Thrust-related anticlines grew progressively from initial layer-parallel shortening, to décollement folding, thrust-tip folding and eventually thrust-ramp folding. Thrust ramps nucleated in the central sector of the overturned forelimb of décollement folds, as a consequence of limb thinning. Thrust-tip folding occurred during outward migration of the ramp tips. The fault-propagation rate was greater at the lower ramp tip, which quickly joined the basal thrust flat, while folding continued beyond the upper tip. The development of the analogue model thrust fault-related folds by progressive changes in kinematics, from décollement folding to thrust-tip folding and finally thrust-ramp folding, compares well with analyses of naturally occurring thrust fault-related folds.

INTRODUCTION

Foreland fold-thrust belts commonly display close interrelationships between thrusting and folding (Dahlstrom, 1969) and their geometric and kinematic links have long been recognized (Rich, 1934; Dahlstrom, 1969; Dennis, 1972; Faill, 1973). Thrust-related folding mechanisms can be described by three end-member types, according to the geometric relationships between the faults and the overlying anticlines: folds that develop above layer-parallel thrusts (décollements), folds that develop at the tip of thrust ramps, and folds that develop above non-planar thrusts (Fisher *et al.*, 1992; Fisher and Anastasio, 1994). These three end members can be respectively defined as décollement folding, thrust-tip folding, and thrust-ramp folding.

Well-constrained kinematic models have been developed to describe thrust-related folding, e.g. fault-bend folding (Suppe, 1983), fault-propagation folding (Suppe and Medwedeff, 1984) and detachment (décollement) folding (Jamison, 1987). They respectively describe thrust-ramp folding, thrust-tip folding, and décollement folding. Modifications and variations of these fundamental models have been developed to describe more complex natural fault–fold systems (Jamison, 1987; Chester and Chester, 1990; Mitra, 1990, 1992, 1993; Erslev, 1991; McNaught and Mitra, 1993; Narr and Suppe, 1994; Storti and Poblet, 1994; Epard and Groshong, 1995; Homza and Wallace, 1995; Wickham, 1995; Storti and Salvini, 1996). Many of the kinematic models (Suppe, 1983; Suppe and Medwedeff, 1984) of thrust-related folding imply a self-propagating evolution, in that thrust-related anticlines develop by the same mechanism from the beginning to the end of their life. As a result self-similar folding models and limb rotation models are commonly thought of as contradictory kinematics for fault-related folding. There are, however, kinematic problems in self-similar fault–fold models (Erslev, 1991; McNaught and Mitra, 1993) and many uncertainties in faulting/folding chronologies and axial surface activities. Faulting has been proposed to precede folding (Rich, 1934), to post-date folding (Willis, 1893), or contemporaneous faulting and folding has been proposed (Dahlstrom, 1970). Axial surfaces can migrate (Stewart and Alvarez, 1991; Butler, 1992) or remain fixed (Fisher and Anastasio, 1994) during folding.

Kinematic and geometric models cannot adequately account for the mechanics and rheological features of natural fault-related fold systems. Computer models (Williams, 1980; Braun and Sambridge, 1994; Erickson and Jamison, 1995; Lan and Hudleston, 1995; Liu and Dixon, 1995; Barnichon and Charlier, 1996; Zhang *et al.*, 1996), analogue rock models (Friedman *et al.*, 1980 and references therein; Chester *et al.*, 1991; Couples *et al.*, 1994), physical models using non-Newtonian materials (Cobbold *et al.*, 1971; Stewart and Alvarez, 1991; Fowler and Winsor, 1996), centrifuge models (Mulugeta, 1988; Liu and Dixon, 1991, 1995; Dixon and Liu, 1992), and sandbox models at 1 g (Malavieille, 1984; Lallemand *et al.*, 1992; Liu *et al.*, 1992; Marshak and Wilkerson, 1992; Calassou *et al.*, 1993; Storti and McClay, 1995; Gutscher *et al.*, 1996 and others) have all been used to simulate

natural thrust–fold systems. In particular, scaled physical models provide a very powerful and visual tool to simulate the evolution of rock deformation through time (Ramberg, 1981).

PREVIOUS WORK

The relationships between faulting and folding have been widely investigated by field, theoretical and experimental research. Overall geometries and strain distribution of natural thrust-related anticlines support either *break-thrust* kinematics (Willis, 1893), i.e. *fold-first* kinematics (Heim, 1919; Wiltschko and Eastman, 1983; Fisher *et al.*, 1992; Woodward, 1992; Fisher and Anastasio, 1994; Morley, 1994), or *fault-first* kinematics (Rich, 1934; Fox, 1959; Royse *et al.*, 1975; Suppe, 1983; Medwedeff, 1989; Hedlund *et al.*, 1994; Jamison and Pope, 1996), and also *contemporaneous folding and faulting kinematics* (Dahlstrom, 1970; Brown and Spang, 1978; Williams and Chapman, 1983; Chester and Chester, 1990; Suppe and Medwedeff, 1990; Alonso and Teixell, 1992; Couzens and Dunne, 1994; Tavarnelli, 1994). McNaught and Mitra (1993) proposed a transition from initial décollement folding to thrust-tip folding, in order to prevent space problems at the lower ramp hinge where a footwall syncline generates, and to maintain a constant PR/SR ratio (fault propagation to fault slip ratio) during deformation. The role of premonitory shear zones (kink bands) in controlling the orientation of fault ramps has been emphasized by Johnson (1995).

In analogue experimental thrust studies Marshak and Wilkerson (1992) described initial lateral compaction, followed by simultaneous slip along the cross-sectional trace of newly formed discrete shear surfaces (thrust ramps). Layer-parallel shortening preceding box folding has also been described in sandbox models by Mulugeta and Koyi (1992) and Koyi (1995). The forelimb of their experimental anticlines then sheared and localized a thrust ramp. Thinning of the forelimb during shearing or rock slice experiments has been documented by Friedman *et al.* (1980).

Experiments by Liu and Dixon (1991, 1995), Dixon and Liu (1992) and Verschuren *et al.* (1996) produced results that support the *fold-first* kinematic model. In particular, Dixon and Liu (1992) have described centrifuge models using viscous–plastic materials where the progressive transition from décollement folding to thrust-tip folding and, finally, to thrust-ramp folding occurred. Layer-parallel shortening affected all of the competent units during contraction. In these models the systematic spacing of thrust ramps was inherited from early buckle folds. Thrust ramps nucleated at the base of the competent units and propagated upward (Liu and Dixon, 1991, 1995; Dixon and Liu, 1992).

A different evolution for thrust-related anticlines was described by Chester *et al.* (1991) in non-scaled rock models. They showed the transition through time from thrust-ramp folding to thrust-tip folding. Moreover, in their experiments thrust ramps nucleated in the central region of the rock slice sandwich as isolated fault segments in the stiffer units, and then propagated upward and downward during subsequent fold growth.

The problem of thrust-ramp nucleation and propagation has also been addressed in theoretical analyses. Gretener (1972) first provided a mechanical explanation of ramp nucleation above the basal décollement, and this was further developed by Eisenstadt and De Paor (1987) and Goff and Wiltschko (1992). Numerical models (Liu and Dixon, 1995; Goff *et al.*, 1996) support décollement folding as a mechanism to localize thrust ramps. Finite element models by Braun and Sambridge (1994) support a fault-propagation folding (Suppe and Medwedeff, 1984) kinematic model. Thrust ramps nucleated at velocity singularities in the base of the models, and then propagated upwards.

In this paper we present results of high-resolution scaled sandbox models designed to investigate the kinematics of thrust-related folds in the brittle field. Detailed analysis of the experimental results has allowed us to propose a kinematic model for brittle thrust-related folds where contractional structures evolve progressively from layer-parallel shortening, to décollement folding, thrust-tip folding, and finally to thrust-ramp folding.

EXPERIMENTAL METHOD

The experimental apparatus used was a glass-sided deformation rig with internal dimensions (length, width, height) of $150 \times 20 \times 20$ cm (Fig. 1). Dry cohesionless 190 μm grain size quartz sand (coefficient of friction $\mu = 0.55$; McClay, 1990a; Liu *et al.*, 1992) and dry 300 μm vermiculite mica flakes (coefficient of friction $\mu = 0.37$, Liu *et al.*, 1992) were used to simulate the brittle deformation of anisotropic sedimentary rocks in accretionary prisms and thrust wedges. Friction against the glass sidewalls was reduced to negligible effects by carefully coating the glass with a transparent, low-friction polymer.

An initial sandpack, 50 cm long $\times$ 20 cm wide $\times$ 2.5 cm thick consisting of alternating 1 mm thick layers of coloured and white sand with thin interlayers of mica flakes (designed to promote bedding-parallel slip; McClay, 1990b), was constructed in the apparatus using an automated sieving machine. Two sets of multilayers were constructed, with different stratigraphy. In the first set, all the sand layers were 1 mm thick, designed to simulate a sequence with constant bed thickness. The second set also consisted of 1 mm thick layers but with four of the layers being 2 mm thick, to simulate a sequence with variable bed thickness. These thicker layers were also expected to be slightly stiffer during deformation. The pre-kinematic stratum at the top of all models consisted of a 5 mm thick black sand layer. In the

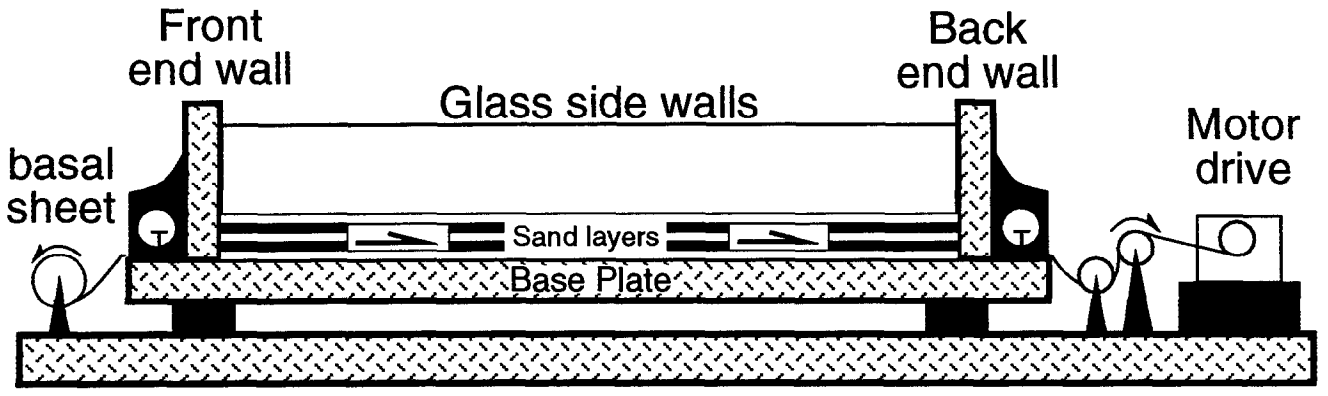

Fig. 1. Diagram of the experimental apparatus (after Liu *et al.*, 1992).

constant bed-thickness sandpacks thin layers of mica flakes were also sieved at 1 mm intervals within this top black unit whereas mica layers were not placed within this upper black unit of the variable bed-thickness sandpacks.

Using a linear scaling factor of 10^{-5} (McClay, 1990b), 1 cm in the models represents approximately 1 km in upper crustal rocks. The models were deformed by moving a horizontal décollement sheet of drafting film (coefficient of friction $\mu = 0.47$; Liu *et al.*, 1992) underneath the multilayer at a constant displacement rate of 6 mm min^{-1}. The backstop was the vertical wooden end of the deformation rig (Fig. 1). Deformation of the sandpack occurred by underthrusting producing a critically tapered Coulomb wedge similar to those produced in other sandbox modelling experiments (Liu *et al.*, 1992; Lallemand *et al.*, 1992; Calassou *et al.*, 1993). All the experiments were recorded using time-lapse photography (1 frame every 2 mm of contraction). After each cm of contraction, syntectonic sediments were added on the active frontal anticline in the thrust wedge. The surface taper of the syntectonic sediments was fixed at about 2°, to simulate the mean depositional angle of marine, terrigenous sediments. This angle also determined the ratio between the thickness of the growth strata close to the forelimb of the frontal anticlines and the syntectonic bed lengths. Different sedimentation rates from no sedimentation to a high sedimentation rate that completely buried the thrust wedge were used in different experiments (Storti and McClay, 1995). This paper analyses in detail the fault–fold relationships in the models where the syntectonic sedimentation rate was lower than tectonic uplift such that emergent thrusts with ramp–flat trajectories were developed.

Completed models were preserved and serially sectioned. Deformation observed through the glass sidewalls of the models was found to be representative of the internal deformation within the models. All the experiments have been repeated at least twice with reproducible results.

RESULTS

In all the experiments a critically tapered Coulomb thrust wedge developed with thrust-related anticlines forming in a piggy-back sequence and progressively younger structures nucleating forelandward of the older ones (see Figs 2 & 3). Three thrust-related folds developed in each experiment before a stable critically tapered Coulomb wedge formed and slid along the décollement with no further internal deformation. The first two anticlines nucleated close to the backstop, whereas the third, long-lived structure developed within the foreland and accounted for most of the total shortening (see Figs 2 & 3). This partitioning of the growth of thrust wedges into an initial stage of fast nucleation of small thrust-related folds close to the backstop, followed by a second stage where much wider, long-lived structures develop, has been well documented in other Coulomb wedge experiments (Liu *et al.*, 1992; Mulugeta and Koyi, 1992; Storti and McClay, 1995).

The thrust fault-related folds found in two experiments (F-6 and F-5) are described in detail below. Model F-6 is a constant thickness multilayer model whereas F-5 is a variable thickness model.

Experiment F-6: constant bed-thickness multilayer

Figure 2 shows the progressive evolution of experiment F-6 in six stages from 6 mm to 90 mm of contraction and Fig. 3 shows the equivalent line diagram interpretations. The progressive development of anticlines I–III were analysed in detail by measuring the maximum bed dip of every discernible layer in the forelimb of each fold (the lowermost layers were highly sheared and details were obscured). Figure 4 shows the fold profiles and plots of bed dip (measured anticlockwise) versus shortening for the three anticlines for 5×4 mm increments of contraction.

All three folds show similar features during their nucleation and development (Fig. 4). The first few mm

of contraction produces layer-parallel shortening without noticeable folding. This is followed by initial formation of the kink-like folds by nucleation and layer rotation in the central and upper sections of the sandpacks (Fig. 4a, f & m). Initial rotation of the layers produces thickening of the steep limb (Fig. 4b, g & n). After a further 4 mm of contraction individual layers have become more highly rotated and the kink band folds have propagated both up to the surface of the model and down to the base of the sandpack (Fig. 4b, g & n). The axial surfaces of these kink band folds dip at angles between 32° (anticline I) and 24–26° (anticlines II and III). The layers are overturned in the central and upper sections of the model whereas they form décollement folds at the base of the sandpack (Fig. 4b, g & n). At these stages the overturned layers in the central sections of the model begin to thin. The next 4 mm of contraction produces further rotation of individual layers in the sandpack such that the maximum dips approach 135° (Fig. 4c, h & o). At these two stages of deformation the two uppermost pre-kinematic layers in anticlines I and II show slightly greater dips that those layers immediately below. A further two increments of deformation for anticlines I and II produce stable kink band geometries with maximum dips of approximately 135° for all layers in the models with the exceptions being the uppermost pre-kinematic layers having greater dips as a result of shearing produced by gravitational collapse of the upper surface of the model (Fig. 4d, e, i & l). Once stable kink band geometries were attained, layer-parallel shortening developed in the foreland. Further displacement produced thinning of the overturned limb of the kink band anticlines such that individual layers became disrupted (Fig. 4e, l & q).

Anticline III in experiment F-6 developed a throughgoing, 24° dipping thrust fault in the increments between 54 mm and 90 mm of contraction (Figs 2f, 3f & 4q). The thrust fault developed from the thinned overturned fold limb thus producing a hangingwall anticline and a footwall syncline (Fig. 4q). The thrust fault becomes flat in the upper part of the model where it is emergent and overrides the syn-kinematic sediments deposited upon the growing wedge (Fig. 4q). The pre-kinematic strata in the hangingwall of the thrust fault are overturned forming a recumbent anticline which was carried up and over the syn-kinematic strata.

Figure 5 shows the progressive evolution of the fold–fault systems for anticlines I–III. Figure 5(a–c) shows the progressive rotation of three key layers in each fold. Note that all rotate to stable orientations of approximately 135° but in all three anticlines the central layers rotate more quickly and reach their final orientation more quickly whereas the lowermost layers rotated more slowly. Individual anticlines became locked when the layers attained their stable orientations and deformation stepped forward as the next fold nucleated in sequence in front of the older, locked structure. In all three folds the forelimb length (i.e. the spacing between axial surfaces) appears to increase linearly with increased shortening (Fig. 5d–f). The displacement–distance diagram (Ellis and Dunlap, 1988) for anticline III after 90 mm of shortening shows maximum displacement in the central section of the model (Fig. 6). This supports the observation that the deformation nucleated here and then propagated both up- and down-section with the first thrust breaks also being found in the centre of the model.

The above analysis shows that all three anticlines in experiment F-6 developed in a similar fashion from initial shortening, followed by décollement folding at the base of the model with kink band development with rotation of the overturned kink band limb to a stable dip of approximately 135°. Further deformation led to thinning of this overturned limb and ultimately to the development of a throughgoing thrust fault nucleating in the central section of the anticlines (Fig. 4q). In the more external anticline (anticline III), further deformation led to fault breakthrough and the fold was translated toward the foreland along a ramp–flat thrust trajectory, thus undergoing additional deformation by thrust-ramp folding.

Experiment F-5: variable bed-thickness multilayer

Figure 7 shows the progressive evolution of experiment F-5 in six stages from 8 mm to 54 mm of contraction and Fig. 8 shows the equivalent line diagram interpretations. The progressive development of anticlines I and II were analysed in detail by measuring the maximum bed dip of every discernible layer in the forelimb of each fold (the lowermost layers were highly sheared and details were obscured). Figure 9 shows the fold profiles and plots of bed dip (measured anticlockwise) versus shortening for the two anticlines in five increments of 4 mm of contraction for anticline I and 5 × 6 mm increments of contraction for anticline II.

Both folds show similar features during their nucleation and development (Fig. 7). The first few mm of contraction (not illustrated) produces layer-parallel shortening without noticeable folding in the region where the fold subsequently developed. This is followed by initial formation of the kink band folds by nucleation and layer rotation in the central and upper sections of the sandpacks (Fig. 9a & g). Anticline I has a box fold geometry as a result of the development of a second hinterland vergent kink band (Fig. 7b & c). Initial rotation of the layers produces thickening of the steep limb (Fig. 9b & h). After a further increment of contraction individual layers have become more highly rotated and the kink band folds have propagated both up to the surface of the model and down to the base of the

Fig. 2. Sequential photograps of experiment F-6, formed against a vertical backstop at the right-hand end of the model. (a) 6 mm contraction. (b) 14 mm. (c) 22 mm. (d) 30 mm. (e) 54 mm. (f) 90 mm.

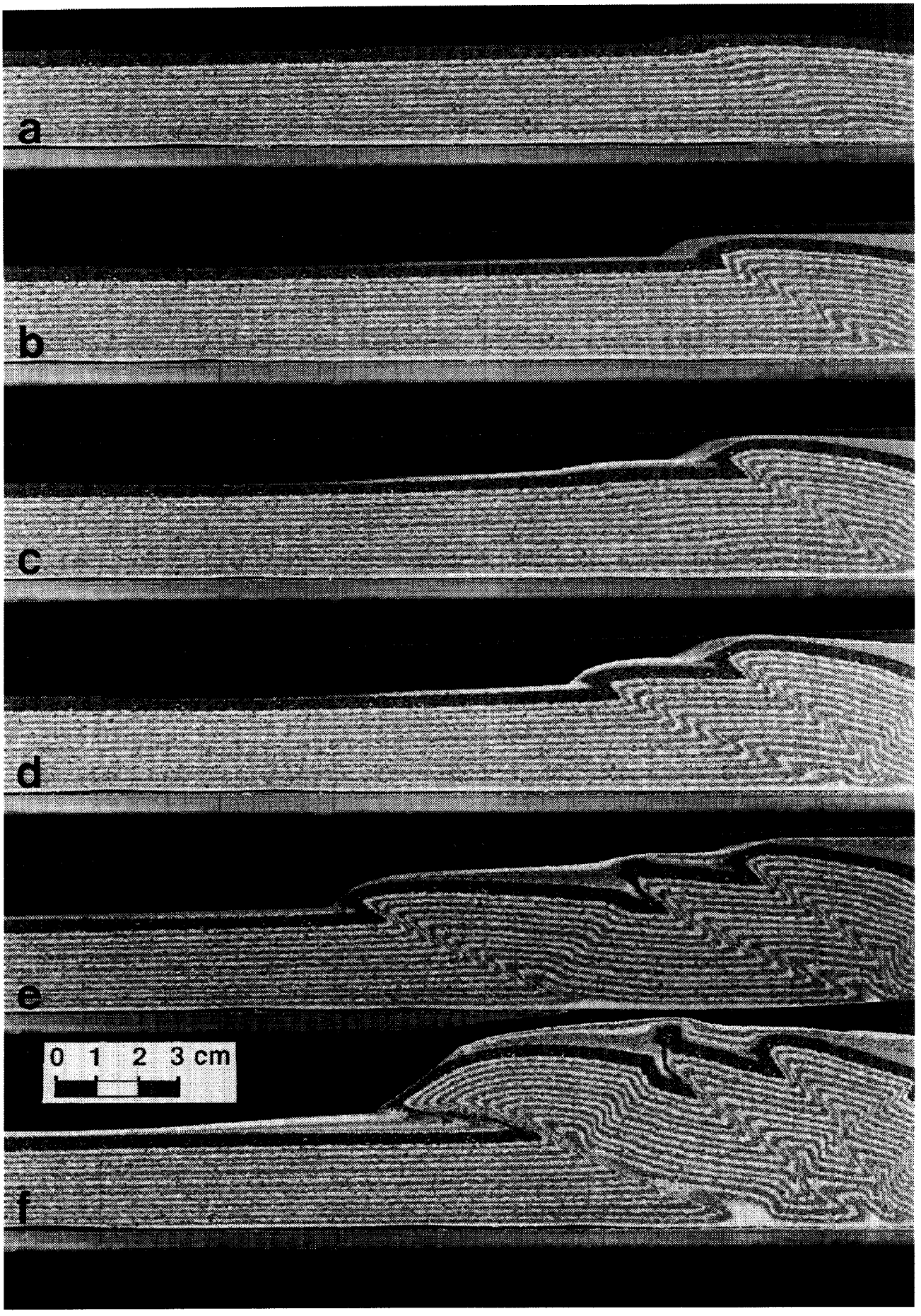
a
b
c
d
e
f
0 1 2 3 cm

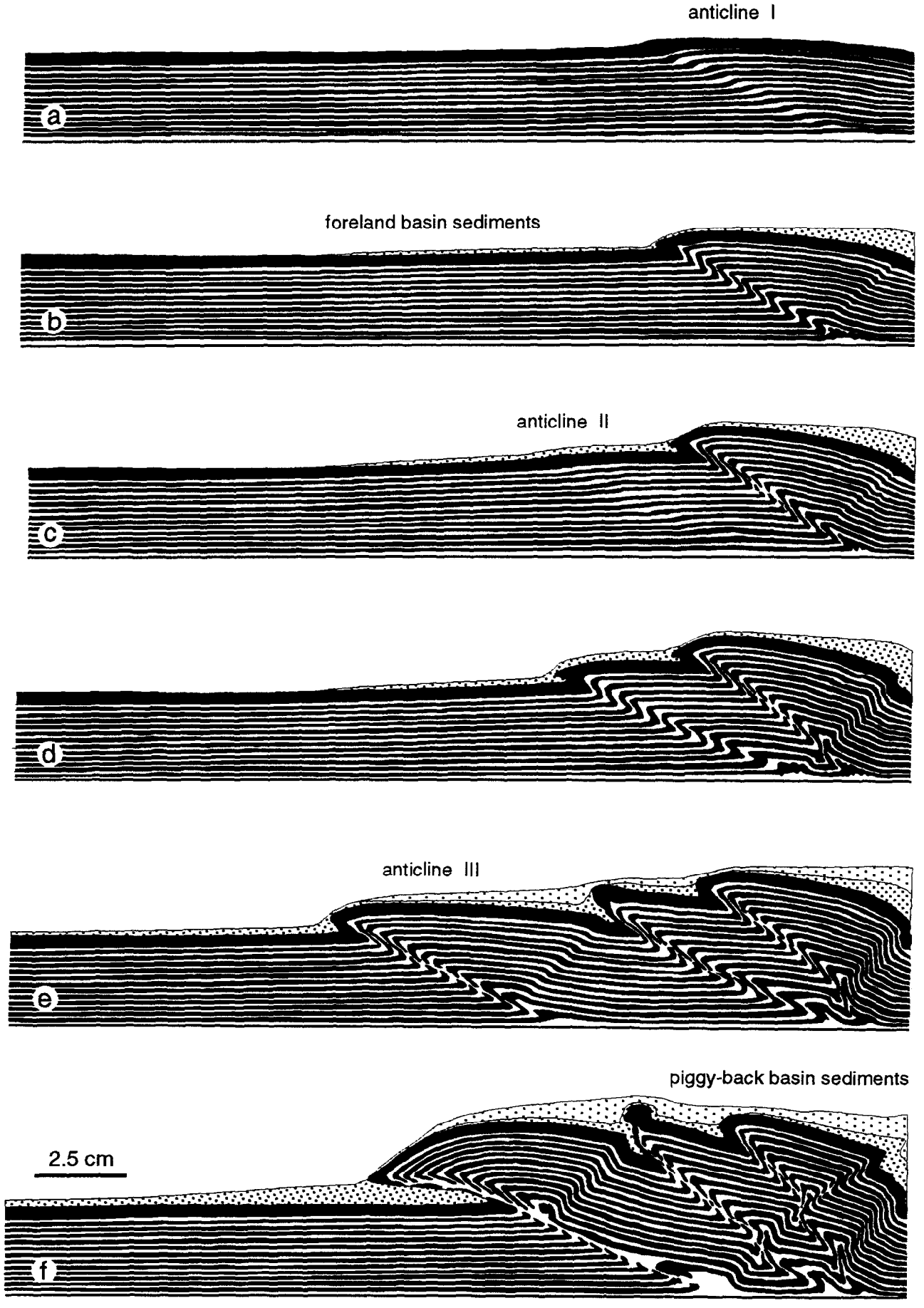
anticline I
a
foreland basin sediments
b
anticline II
c
d
anticline III
e
piggy-back basin sediments
2.5 cm
f

sandpack (Fig. 9b & h). The axial surfaces of these kink band folds dip at angles between 28° (anticline I) and 17° (anticline II). In contrast to experiment F-6 (constant-thickness multilayer) the dip distributions are more irregular in the variable bed-thickness multilayer (F-5) with some elements of disharmonic folding along the axial surface of the kink-band folds (Fig. 9c, h & i). The layers are overturned in the central and upper sections of the model whereas they form décollement folds at the base of the sandpack (Fig. 9b & h). The next increment of contraction produces further rotation of individual layers in the sandpack such that the maximum dips approach 135° (Fig. 9c & i). At this stage of the deformation the central layers in the kink band begin to undergo thinning. A further two increments of deformation for anticlines I and II produce stable kink band geometries with maximum dip of approximately 135° for all layers in the model. Anticline I has a more box-like form with décollement folding at the base of the sandpack (Fig. 9e). Development of stable kink band geometries favoured layer-parallel shortening in the foreland of the anticlines, contemporaneous with ramp nucleation in the central sector of the forelimb. As in experiment F-6, with increased contraction, a third anticline developed far from the backstop, and then underwent fault breakthrough as a large thrust sheet developed.

Figure 10 shows the progressive evolution of the fold–fault systems for anticlines I and II. Figure 10(a & b) shows the progressive rotation of three key layers in each fold. Note that all rotate to stable orientations of approximately 135° but in both anticlines, the central layers rotated more quickly and reach their final orientation more quickly whereas the lowermost layers rotated more slowly. Individual anticlines become locked when the layers attained their stable orientations and deformation stepped forward as the next fold nucleated in sequence in front of the older, locked, structure. In both folds the forelimb width appears to increase linearly with increased shortening (Fig. 10c & d).

The above analysis shows that the two anticlines in experiment F-5 developed in a similar fashion from initial shortening, followed by décollement folding at the base of the model with kink band development with rotation of the overturned kink band limb to a stable dip of approximately 135°. In contrast to experiment F-6 the presence of the thicker stiffer layers produced greater initial variations in maximum limb dips in the forelimb of the folds and stable (approximately 135°) dips were only attained at high values of shortening in each fold.

EVOLUTIONARY MODEL

The detailed observation and analysis of the progressive development of thrust-related folds in the sandbox models has enabled an evolutionary model to be developed (Fig. 11). Stage 1 of this model has décollement folding roughly above the arrested fault tip on the basal décollement (Fig. 11a) with folding and shortening in the section above the fault-tip line. The décollement folding is characterized by kink band folds. With increased shortening the layers rotate within the kink bands to become overturned (dips around 135°) and a thrust fault nucleates in the central section of the model (Fig. 11b). Contemporary, layer-parallel shortening occurs in the foreland. The fault in this position propagates both up and down the overturned limb of the kink band (Eisenstadt and De Paor, 1987) until it coalesces with the horizontal thrust at the base of the model (Fig. 11b & c). The thrust now has a ramp–flat trajectory (Fig. 11c). Increased contraction occurs by propagation of the thrust up-section with thrust-tip folding ahead of the upper tip line (Fig. 11c) until breakthrough occurs and the thrust becomes emergent onto the upper surface of the model forming an upper flat (Fig. 11d). The thrust has now developed a flat–ramp–flat trajectory with thrust-ramp folding above the kinks in the thrust surface. In detail, during the development of the ramp section of the thrust, individual layers are first thickened as they rotate under a hinge-parallel shear couple (Fig. 12a) and then with increased deformation become overturned and thinned (Fig. 12b).

The kinematic path as outlined in Fig. 11 can be divided into two main stages: (a) a first stage of limb rotation, and (b) a second, longer-lived stage characterized by self-similar kink band and thrust-ramp folding. Limb rotation occurs during décollement and thrust-tip folding, where also the forelimb length increases (i.e. axial surface migrates), while the limb dip does not change significantly during further forward translation of the anticline by thrust-ramp folding. This means that in this model, self-similar folding and limb rotation are not contrasting kinematics, but instead they characterize two different stages of the same evolutionary path. In particular, folding develops self-similarly for most of the evolution of a thrust-related structure, after a short initial stage of limb rotation. In fact, in the experiments limb rotation generally occurred only in the first 6–8 mm of contraction for each structure, compared to the final displacement achieved by a typical thrust sheet far from the backstop (12–15 cm, Liu *et al.*, 1992; Koyi, 1995; Storti and McClay, 1995).

Such a model as outlined in Fig. 11 is in agreement with the experimental observations and permits the development of both hangingwall recumbent anticlines and footwall synclines as found in many natural examples of thrust-related folds. This model is also in good agreement with experimental results obtained by Dixon and Liu (1992) and Liu and Dixon (1995) in centrifuge models using viscous–plastic analogues.

Fig. 3. Line drawings of sequential photographs in Fig. 2 (model F-6).

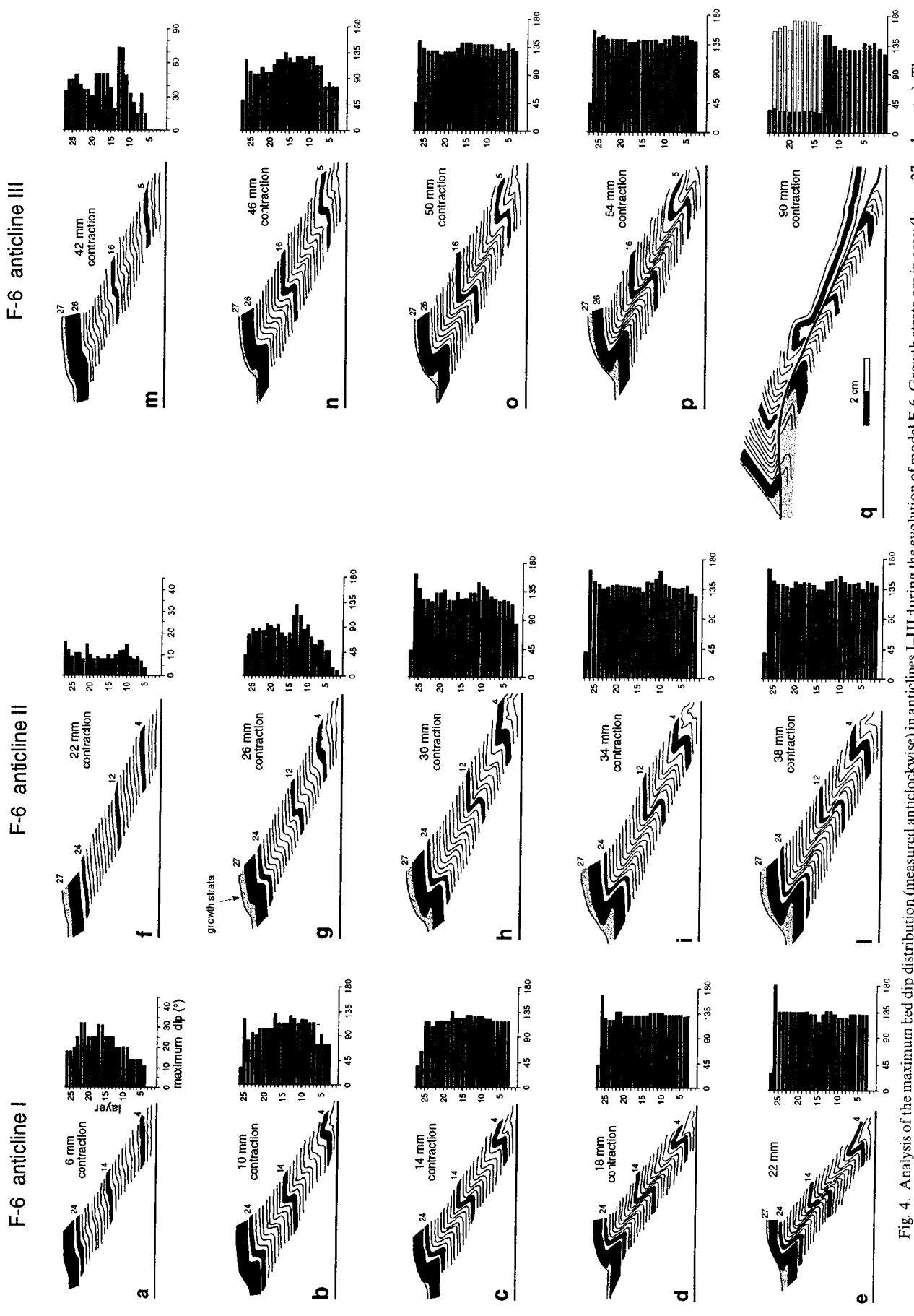

Fig. 4. Analysis of the maximum bed dip distribution (measured anticlockwise) in anticlines I–III during the evolution of model F-6. Growth strata are in gray (layers 27 and greater). The black beds are used as reference layers in the graphs of Fig. 5. In (q) black bars show the dip of the strata in the footwall syncline, white show the refolded, recumbent strata in the hanging wall, and gray indicates the right-way-up panel of the same strata, above the recumbent panel.

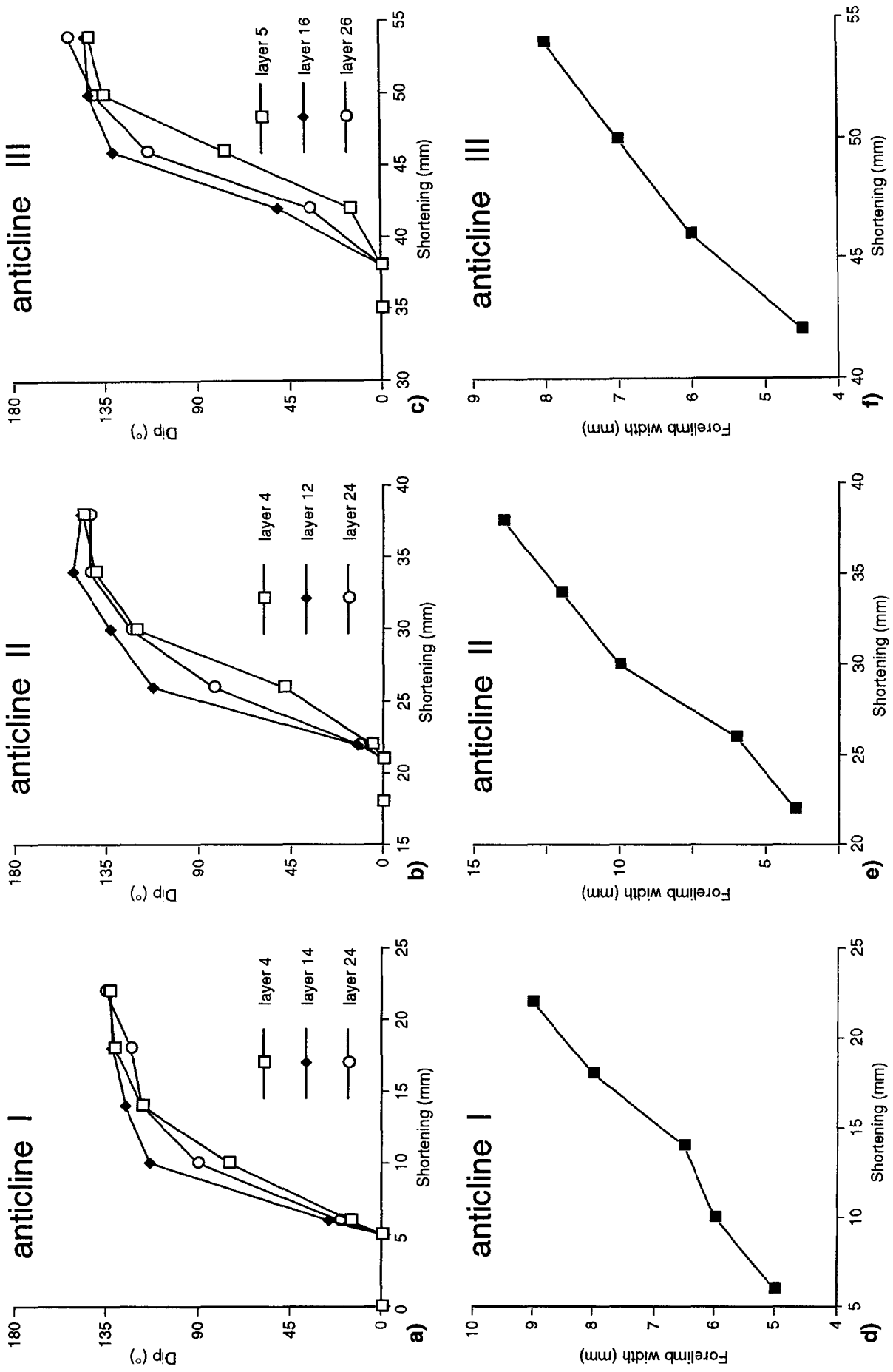

Fig. 5. Progressive evolution of the dip of three selected layers (a, b, c) and forelimb widening with increasing contraction (d, e, f) during the growth of the experimental anticlines in model F-6. Graphs (a) and (d) refer to the first anticline, (b) and (e) refer to the second anticline, (c) and (f) refer to the third anticline.

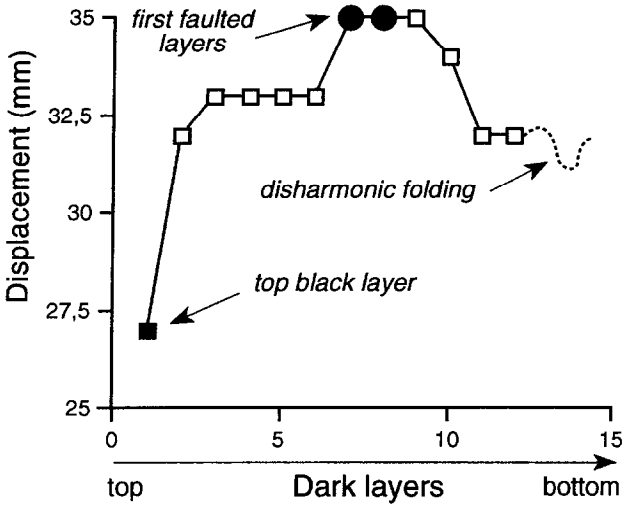

Fig. 6. Displacement–distance diagram for the final stage of model F-6 (Fig. 3f). Displacements are calculated for the top layer and dark (blue) layers, from the top to the bottom of the sandpack. The lowermost layers were highly sheared and disharmonically folded, and details were obscured. Displacements are calculated for corresponding layers in the footwall syncline and in the hangingwall anticline.

MECHANICAL INSIGHTS

Ramp nucleation in the central sector of the experimental kink bands can be mechanically predicted by considering both the contribution of the stress components acting during the folding process and the strength of the material (Fig. 13). The experimental sandpack experiences a stress field that is generated by the basal pull and the gravitational loading. Since the particle paths remain almost parallel to the glass walls (i.e. to the contraction direction, see Fig. 7), the mechanics of the experiments can be fully described in a two dimensional space. Graphs in Fig. 13 illustrate the values of the main discussed variables through the sandpack.

The vertical component (σ_v) of the gravity-induced stress (maximum stress) is given by:

$$\sigma_v = \rho g h \tag{1}$$

where ρ is the average density of the sandpack (1580 ± 1 kg m^{-3}; Liu *et al.*, 1992) and g is the acceleration of gravity (9.8 m s^{-2}). Considering the overall flat shape of the sand volume, this vertical stress will not produce appreciable deformation along the horizontal axes. Thus a horizontal stress component is present, and can be computed by the uniaxial strain law (Turcotte and Schubert, 1982). The horizontal component of the stress induced by gravity (σ_h) will be:

$$\sigma_h = \frac{\sigma_v \nu}{1-\nu} = \frac{\rho g h \nu}{1-\nu} \tag{2}$$

where ν is the Poisson's ratio for the used sand. In the following we have used a constant value for ν of 0.3 (Turcotte and Schubert, 1982) through all the sandpack.

The basal pull (P) exerts a horizontal stress (σ_p) to the sand. The horizontal stress (σ_p) will generate a negligible vertical stress component, due to the overall flat shape of the sandbox experiment and the unconstrained top surface of the sand (i.e. uniaxial stress conditions). The horizontal stress component induced by the basal pull (σ_p) will attenuate along the vertical co-ordinate (h), which is zero at the top and increases toward the bottom, in the sandpack of thickness s, from a maximum value at the bottom (almost equal to the pull) to absent at the very top of the sand multilayer. Due to the attenuation in the propagation through the sandpack of the basal pull applied to the bottom, this component of the horizontal stress (σ_p) will progressively decrease towards the top of the multilayer, where it reduces to zero (Mandl, 1988; Barnichon and Charlier, 1996). In order to replicate this behaviour, the path of the (horizontal) stress component induced by the basal pull through the sandpack has been represented as the combined result of a constant decreasing function (df_1) with a second order attenuation one (df_2). That is:

$$df_1 = Ph_r \tag{3}$$

$$df_2 = -Ph_r(h_r - 2) \tag{4}$$

$$\sigma_p = f df_2 + (1-f) df_1 \tag{5}$$

where f is the fraction (from 0 to 1) of deviation from the linear attenuation df_1, and h_r is the depth relative to the thickness s.

In order to understand the role of the basal pull and of the gravity in the failure process, it is convenient to separately compute the shear stress components induced by each of them. The basal pull component of the shear (τ_p) on a surface that dips at an angle θ follows from the equation of the shear stress in a two dimensional system:

$$\tau_p = 1/2 \sigma_p \sin 2\theta \tag{6}$$

The gravity-induced shear (τ_g) will be:

$$\tau_g = 1/2(\sigma_h - \sigma_v)\sin 2\theta \tag{7}$$

The resulting total shear stress (τ) along the plane will be the sum of these two components:

$$\tau = \tau_p + \tau_g \tag{8}$$

Note that the two components have an opposite sense of shear, for $\sigma_v \geq \sigma_h$. This is evident in Fig. 13(a), where the basal pull shear (τ_p) curve has greater values with respect to the corresponding total shear (τ) curve.

The experimental kink bands are the more favourable breakage surfaces and show an average dip (θ^*) of about 24°. Thus we will compute the normal and shear stress components of the stress field for surfaces with the same

Fig. 7. Sequential photographs of experiment F-5 formed against a vertical backstop at the right-hand end of the model. (a) 8 mm contraction. (b) 20 mm. (c) 28 mm. (d) 42 mm. (e) 54 mm.

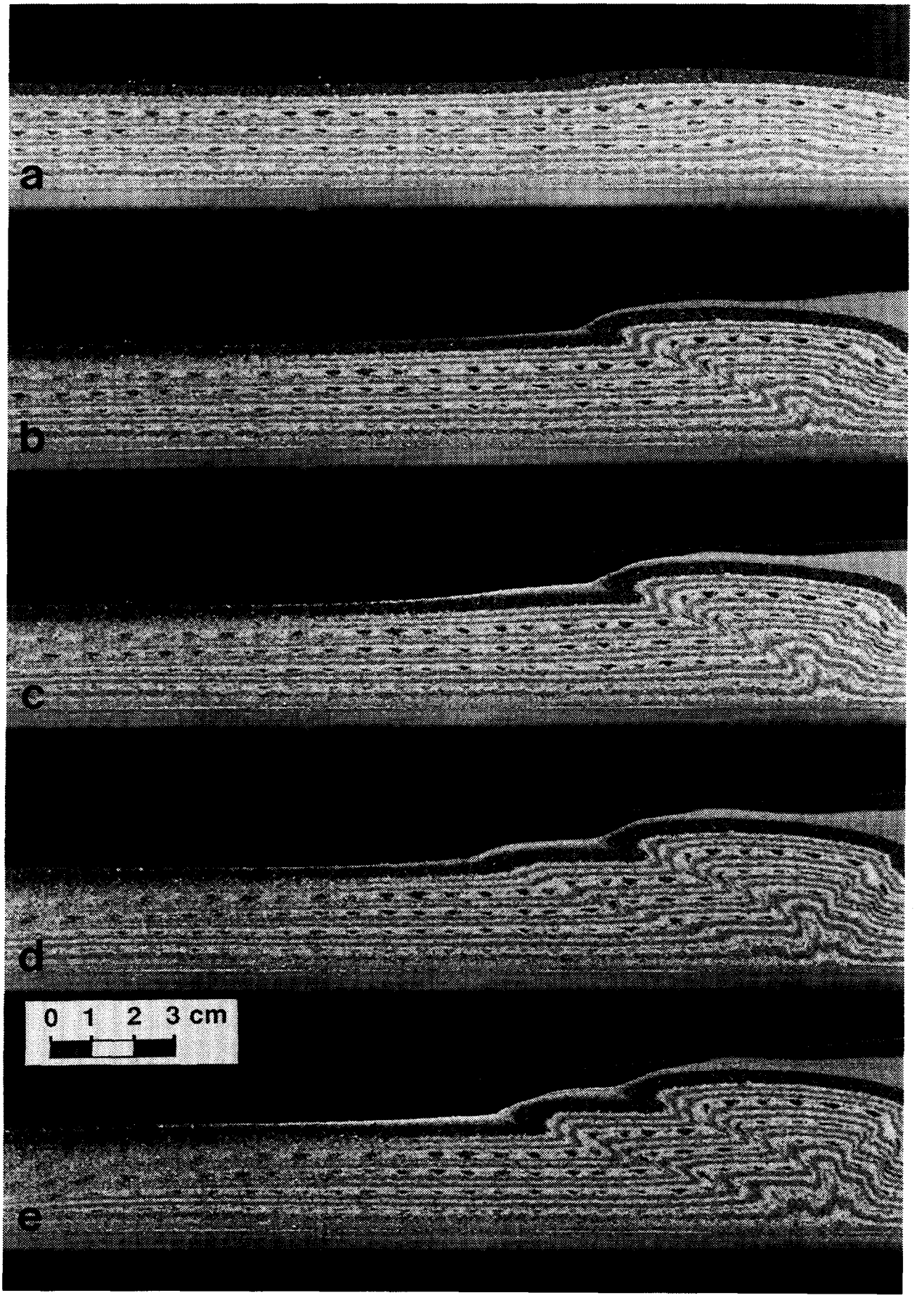
a
b
c
d
e
0 1 2 3 cm

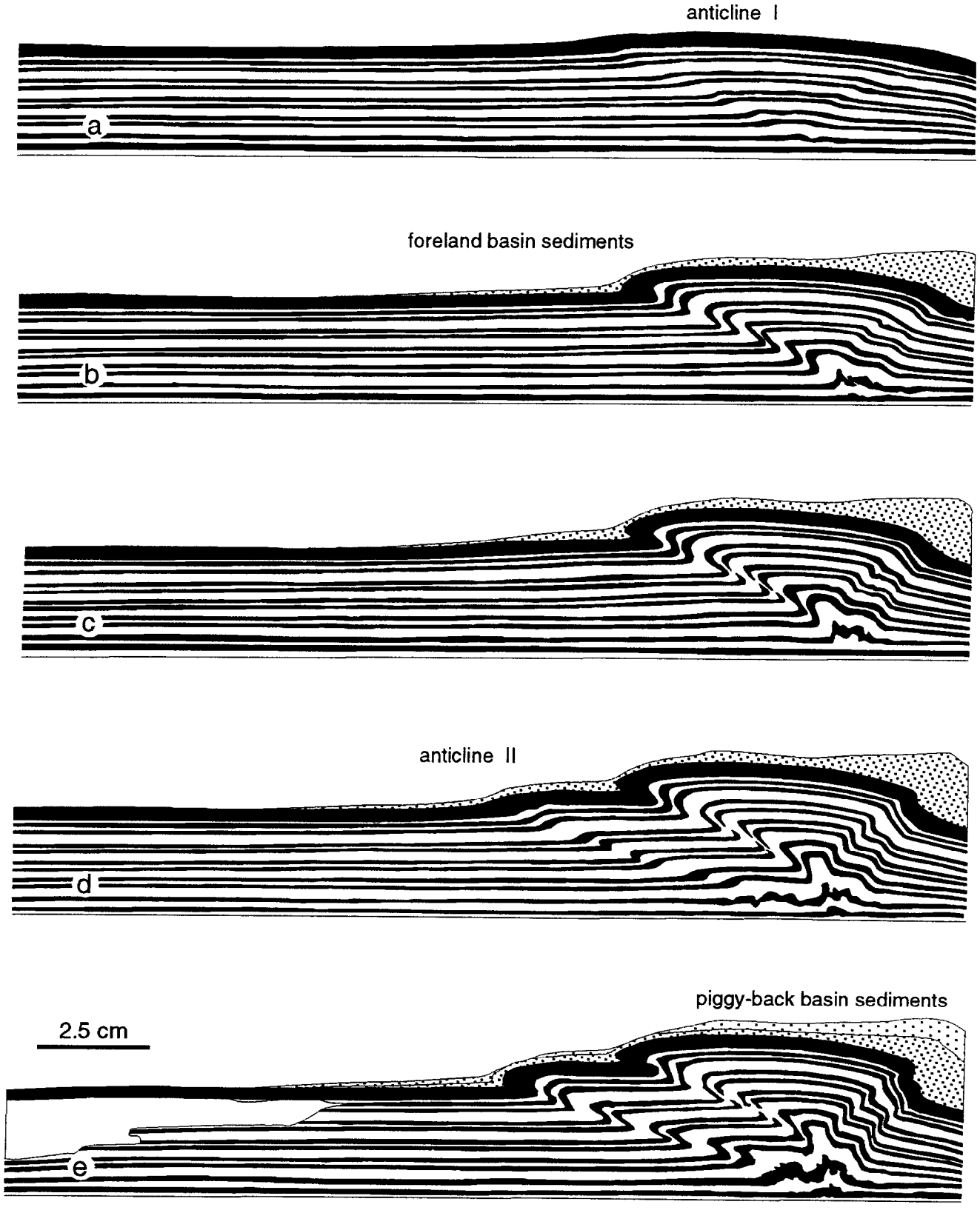

Fig. 8. Line drawings of sequential photographs in Fig. 7 (model F-5).

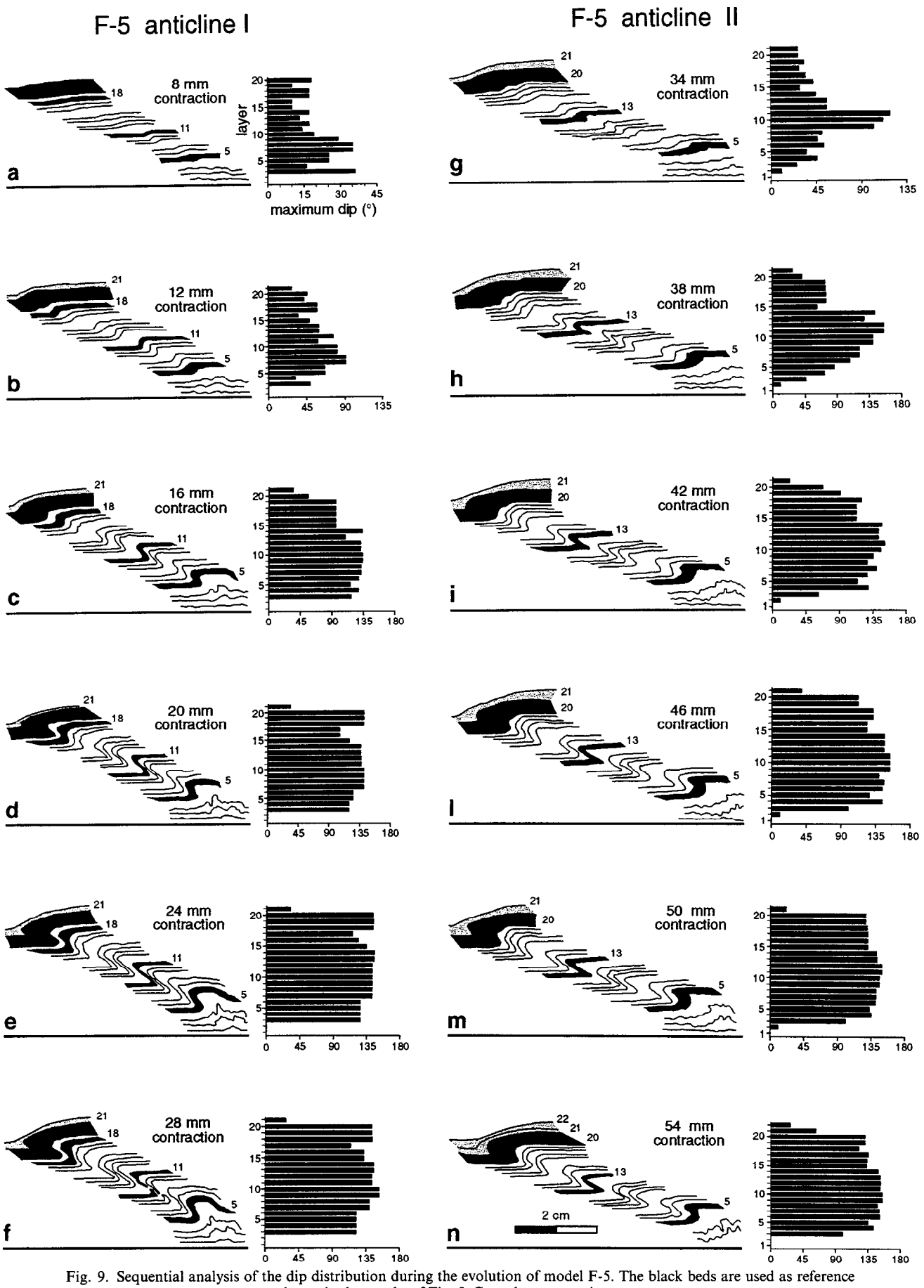

Fig. 9. Sequential analysis of the dip distribution during the evolution of model F-5. The black beds are used as reference layers in the graphs of Fig. 5. Growth strata are in gray.

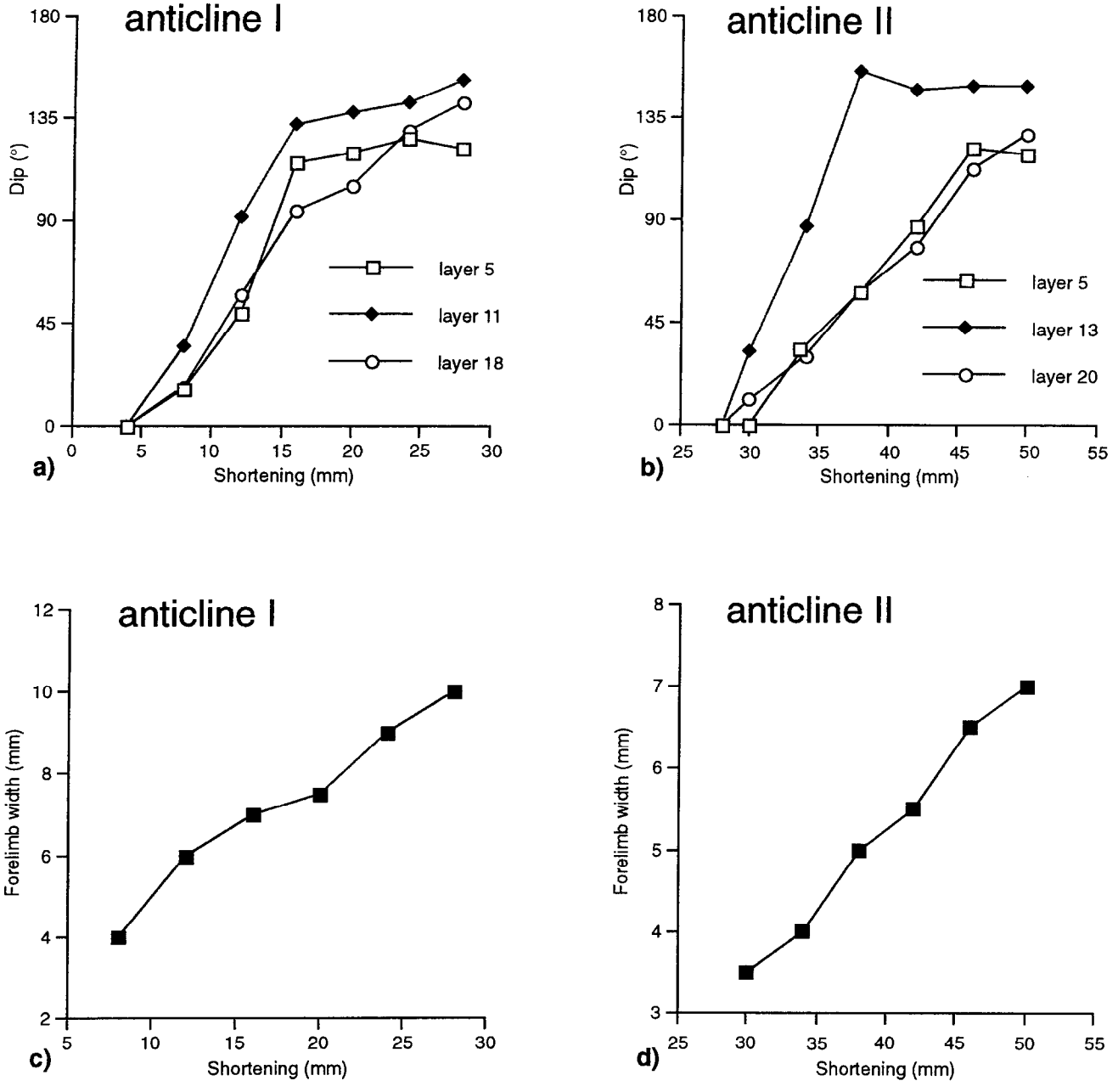

Fig. 10. Progressive evolution of the dip of three selected layers (a, b) and forelimb widening with increasing contraction (c, d) during the growth of the experimental anticlines in model F-5. Graphs (a) and (c) refer to the first anticline, (b) and (d) refer to the second anticline.

dip (θ^*). The total shear (τ^*) along these surfaces is derived by substituting (θ^*) in equations (6) and (7), and substituting them into (8):

$$\begin{aligned}\tau^* &= 1/2\sigma_p \sin 2\theta^* + 1/2(\sigma_h - \sigma_v)\sin 2\theta^* \\ &= 1/2(\sigma_p + \sigma_h - \sigma_v)\sin 2\theta^*\end{aligned} \quad (9)$$

The strength (Σ) of the sandpack along surfaces parallel to the kink plane is given by the Mohr–Coulomb criterion:

$$\Sigma = c_0 + \sigma_n \tan\varphi \quad (10)$$

where φ is the internal friction angle of the sandpack (28.8°), c_0 is the cohesion of the sandpack (about 10 Pa), and σ_n is the component of the stress normal to the plane, and due to the gravity load plus the horizontal pull:

$$\sigma_n = 1/2(\sigma_p + \sigma_h + \sigma_v) - 1/2(\sigma_p + \sigma_h - \sigma_v)\cos 2\theta^* \quad (11)$$

The adopted low value for the cohesion (c_0) derives from considering that its value be almost negligible in unfaulted conditions, due to the relatively small thickness of the sandpack (Mandl, 1988). Nevertheless, it must be higher than zero, otherwise in any experimental conditions failure would always start at the surface of the sandpack, where the strength of the material (Σ) is equal to the cohesion (c_0) (equations 10,

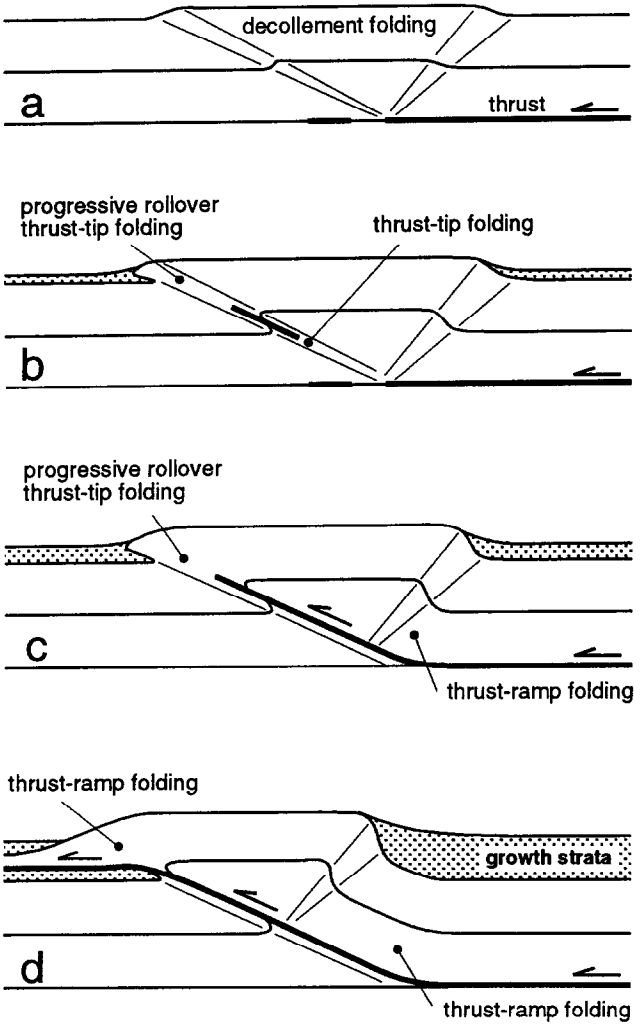

Fig. 11. Conceptual model to show the evolutionary path observed during the growth of the experimental anticlines. Thrust-tip folding at the upper ramp-tip line develops according to the progressive rollover kinematics (Storti and Salvini, 1996).

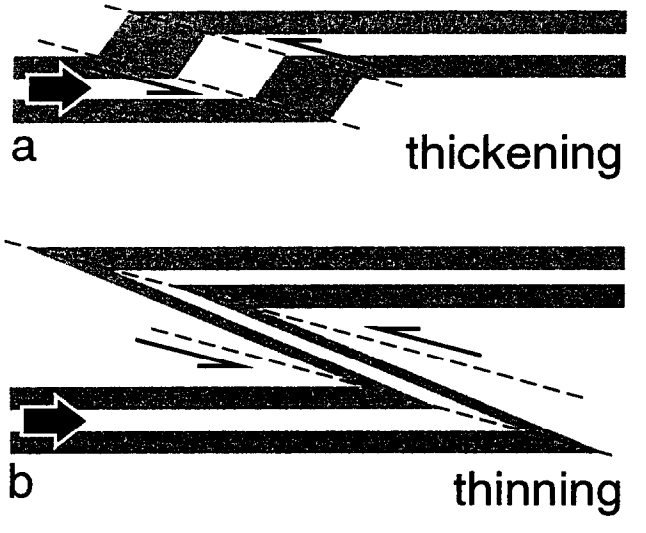

Fig. 12. Thickness changes in a kink band developed by simple shear.

11), but the stress component (σ_p) induced by the pull shear is positive.

Note that from the friction angle we can derive the dip of the theoretical failure plane (θ_t) with the maximum principal stress:

$$\theta_t = 45° - \varphi/2 \tag{12}$$

In our experiment this would result with a theoretical dip of the kink plane (θ_t) of 28.8°, that differs from the observed one ($\theta^* = 24°$). This difference may relate to partial Griffith behaviour (Griffith, 1924) of the sand and/or may have been introduced by the semi-ductile deformational mechanisms in the kink band (i.e. grain rotations). In the following, we will refer to the measured dip of kink planes (θ^*). Failure will be induced along planes dipping at (θ^*) by the progressively increasing pull along the base when the total shear (τ^*) will exceed the strength (Σ). This process is shown in the graph of Fig. 13(b), where the characteristic convex shape of the final equation, the deformation function (D_f):

$$D_f = \tau^* - \Sigma \tag{13}$$

shows that the maximum of D_f falls in the central zone (h^*) of the multilayer. Numbers from 1 to 7 in the three families of curves relate to progressive increments of the basal pull up to failure (curve 6) and fracture widening (curve 7). The family of D_f curves in Fig. 13(b), and in particular curve 7, may resemble the deformation process with increasing contraction. Note that the deformation tends to be distributed asymmetrically around h^* with relatively higher values toward the bottom of the multilayer. Such a distribution means that the amount of deformation at corresponding stages will be greater in the lower sector of the multilayer than in the upper sector. That is, outward migration of the fracture tips will be faster toward the bottom than toward the top of the sandpack. This is in good agreement with the experimental results (Figs 2–9).

The same final D_f function for the critical P^* value of the pull shear (curve 6 in Fig. 13b) appears also in Fig. 13(a). The broad maximum of (D_f) implies that the first irrecoverable deformation will occur within an interval in the central sector of the multilayer, depending on local anisotropies. The position of h^* is a function of the f parameter that has been introduced, responsible for the shape of the pull shear attenuation through the sandpack.

Experimental conditions have been reproduced by computer modelling (Fig. 13a) with the following parameters: $f = 0.145$; $P^* = 980$ Pa, thus resulting $h^* = 0.5$. These values are not critical, and small variations will not influence the overall shape of the curves in Fig. 13, resulting in a shift of the first failure point within the central portion of the sandpack, together with a variation in the concentration of the deformation. The failure point falls inside the sandpack with almost any f value. For the limit case of $f = 1.0$, the distribution of the horizontal stress (σ_b) induced by the basal pull shear follows a second order curve, the failure area falls closer

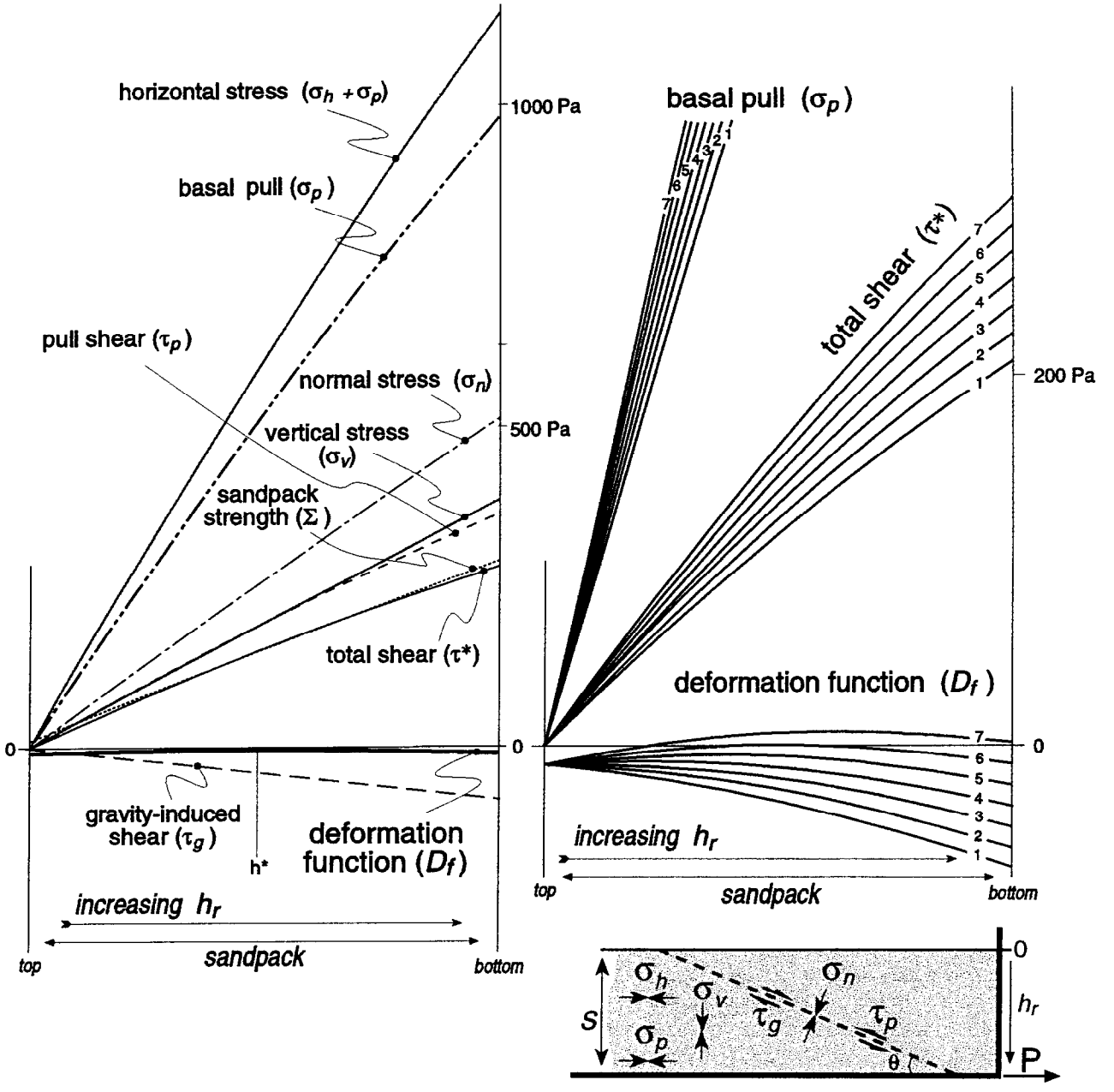

Fig. 13. Computer model of the state of stress during the development of an experimental anticline (a). Note how the sum of the acting stresses has a gentle convex shape, intersecting the x-axis in the central sector (central sector of the sandpack). In (b) the increasing total shear minus the sandpack strength is shown for an increasing pull shear, until the elasticity limit is exceeded in the central sector of the x-axis (central sector of the sandpack).

to the surface of the sandpack ($h^* = 0.113$), and tends to concentrate along the first failure point (h^*). For $f = 0.0$, the stress induced by the pull attenuates following a straight line, and failure starts at the bottom of the sandpack, but with a very poor concentration.

As the above results clearly show, the main factor that leads to the concentration of the stress and deformation in the central portion of the sand multilayer is the distribution of the stress induced by the basal pull through the sandpack. The modelled attenuation strongly relates to the basal pull mechanism adopted in the experiment. Variations in the mechanics of the experiments, as in a back-push apparatus, might produce different stress partitioning, and consequently different failure distribution in the sandpack.

In the physical modelling we have considered the mechanical behaviour of the sand as almost constant through the sandpack. Due to the progressive compaction of the sand multilayer from the top towards the bottom, the Poisson's ratio (v) will slightly increase from the top to the bottom. The addition of a linearly increasing Poisson's ratio (v) (from 0.2 near the surface to 0.3 at the bottom) does not produce significant changes in the overall physical behaviour of the experiment, and results in: (a) a moderate shift of the maximum deformation zone (h^*) towards the bottom of the

sandpack; and (b) a narrower area of deformation around the h^* point.

Both experiments and computer modelling have been carried out under dry conditions. In nature, the presence of a pore fluid pressure would reduce the strength of the material and flatten the shape of the curves in Fig. 13, but it will not greatly change the location of the maximum deformation across the multilayer.

The numerical modelling has been specifically designed to simulate the mechanical and rheological conditions in the sandbox experiments, but also variations of the cohesion and of the internal friction angle will preserve the same overall shape of the curves. This allows the generalization, in thrust-related folding, of our results to the natural behaviour of rocks — i.e. the first failure zone is likely to occur within the central sector of the deformed rock sequence.

DISCUSSION

In our models described above, thrust-related folds nucleated as décollement folds, developed into thrust-tip folds, and finally underwent forelandward translation by thrust-ramp folding. This evolution is similar to that described by Dixon and Liu (1992) and Liu and Dixon (1995) in centrifuge models. Two important innovative features of our results are: (a) thrust ramps nucleated in the central sector of the experimental multilayer; and (b) the kinematic mechanism changed from limb rotation to self-similar folding during the evolution of the thrust-related anticlines.

Thrust ramps nucleated in the forelimb of décollement anticlines (i.e. localized by earlier-stage folds). However, the location of thrust ramps by fold limbs does not necessary imply that folding precedes faulting during the growth of a thrust-related anticline. In fact, in the models, the position of folds was determined by the stick-slip propagation of the fault along the basal décollement (Mulugeta and Koyi, 1992). This is in turn determined by the internal mechanics of the growing thrust wedge (e.g. Davis *et al.*, 1983; Liu *et al.*, 1992; Mulugeta and Koyi, 1992). The basal décollement thrust allowed layer-parallel shortening to occur before the development of the anticlines (Marshak and Wilkerson, 1992), i.e. faulting preceded folding. Even if asymmetric décollement folds localized subsequent thrust ramps, the nucleation and development of the same anticlines was related to the slip along a pre-existing blind décollement. The lack of a direct influence of layering on fold wavelengths in sandbox models, as shown by the variations of fold spacing during shortening (Liu *et al.*, 1992; Mulugeta and Koyi, 1992; Storti and McClay, 1995), apparently contrasts with many field tests of the Biot (1961) buckling theory (Sherwin and Chapple, 1968; Fisher *et al.*, 1992 and references therein). These results highlight how the complex relationships between faulting and folding are oversimplified in the simple conundrum as to whether the macroscopically ductile deformation precedes brittle or vice versa during the growth of thrust-related anticlines.

A significant difference in the fold–fault evolution documented in our experiments and those shown by Dixon and Liu (1992) and Liu and Dixon (1995) lies in the nucleation point and directions of propagation of the thrust ramps. In our models thrust ramps nucleated in the middle of the stratigraphic sequence and propagated both downward and upward. In contrast, Dixon and Liu (1992) documented ramp nucleation at the base of a competent layer and its propagation only occurred upward. This difference may be due to the different experimental techniques and materials.

Thrust-ramp nucleation in the central sector of the experimental multilayer, followed by outward propagation of the fault tips has also been observed by Chester *et al.* (1991) in rock models. However, in their models, thrust-ramp folding preceded thrust-tip folding. These difference may be due to the non-scaled experimental deformation of rock laminates.

In our experiments we were able to document thrust-ramp nucleation in the central sector of the sandpack, and the outward propagation of the fault tips. In contrast, however, Marshak and Wilkerson (1992) inferred simultaneous slip along the cross-sectional trace of the thrust ramp. This difference arises from a difference in resolution between the two sets of experiments. Our models consisted of very closely spaced alternating differently-coloured, thin sand layers and this allowed us to carefully detect the nucleation and subsequent evolution of the thrust ramps. The more homogeneous sandpack used by Marshak and Wilkerson (1992) did not allow comparable details to be observed.

Syntectonic sedimentation

In experiments F-6 and F-5 discussed in this paper the syntectonic sedimentation rate was always lower than the uplift rate of the anticlinal fold crests. Other experiments have also been run where high syntectonic sedimentation rates were used (Storti and McClay, 1995). Where the syntectonic sedimentation rate (S) was increased with respect to the uplift rate (U), i.e. when the U/S ratio became greater than 1 (Storti and Salvini, 1996), the high sedimentary supply favoured the persistence of folding at the upper ramp tip. In contrast to experiments conducted with low syntectonic sedimentation rate, a change in the kinematic mechanism from thrust-tip folding to thrust-ramp folding does not occur, and an upper ramp–flat fault trajectory does not form.

NATURAL EXAMPLES

The results of our sandbox fault-related folds can be compared with similar evolutionary thrust-fold patterns described in the literature. In a detailed study of

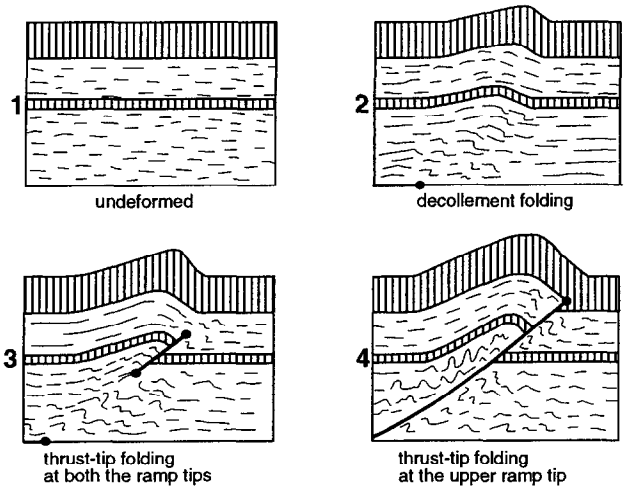

Fig. 14. Evolutionary model for thrust-related folds in the Osen–Røa thrust sheet, Norway. After Morley (1994).

imbricates at the base of the Osen–Røa thrust sheet, in Norway, Morley (1994) proposed an evolutionary model for thrust-related folding which closely resembles our experimentally-derived model before fault breakthrough (cf. Figs 11 & 14). A down-plunge view of the deformed Cambro-Ordovician sequence exposes thrusts passing down-section and up-section into folds. The lateral equivalence of folds and faults suggests that thrusts nucleated within the thrust sheet and propagated both upward and downward (Morley, 1994).

Fault displacement analyses at various scales (from microfaults to regional-scale thrusts) strongly suggest that thrusts initiate above a décollement and propagate both up- and down-section (Ellis and Dunlap, 1988). Hathaway and Gayer (1995) showed this behaviour in the South Wales Variscan Coal Basin. In addition, thrust-ramp nucleation in the central sector of the deformed multilayer has been proposed by balancing seismic reflection sections across the Nankai accretionary prism (Morgan and Karig, 1995). A study of a series of kink bands northwest of Cody, Wyoming, U.S.A., allowed Johnson (1995) to illustrate a similar association of faults and shear zones (kink bands) similar to that which has been observed in our experiments. The transition from unfaulted to faulted kink bands in the same outcrop suggests that the position and orientation of the faults were controlled by the position and orientation of the shear zones (Johnson, 1995). Layer-parallel shortening preceding folding and thrusting has been widely described in foreland fold-thrust belts (Wiltschko *et al.*, 1985; Bowler, 1987; Geiser, 1988; Kilsdonk and Wiltschko, 1988; Tavarnelli, 1994; Yang and Gray, 1994; Butler and Bowler, 1995; Markley and Wojtal, 1996). Layer-parallel shortening has also been observed to precede folding and thrusting in sandbox models (Mulugeta and Koyi, 1992; Koyi, 1995), in centrifuge models (Liu and Dixon, 1990) as well as in finite element models (Erickson and Jamison, 1995).

From the above examples it can be seen that both in experiments and in many natural examples, thrust fault-related folds do not develop solely by a self-propagating mechanism but rather develop progressively with a change in deformation mechanism from layer-parallel shortening, décollement folding, nucleation of the ramp section of the thrust within the folded layer, coalescence of thrust fault components and thrust-tip folding, and finally to thrust-ramp folding.

CONCLUSIONS

Results of detailed sandbox experiments on thrust-related folding have shown that:

(1) during the evolution of thrust-related anticlines the kinematics change from layer-parallel shortening, to décollement folding, to thrust-tip folding and finally to thrust-ramp folding;

(2) thrust-related folds develop by limb rotation, that triggers thickness changes, with initial thickening overprinted by later thinning;

(3) thrust ramps nucleate in the middle of the multilayer, as the ultimate consequence of forelimb thinning in décollement folds; and

(4) the occurrence of stiff layers within the deforming sequence enhances differential rotations in the forelimb of tip folds and disharmonic folding in the anticlinal cores.

Tracking the different kinematic mechanisms of contractional fold growth through time highlights how the current kinematic models of fault-bend folding, fault-propagation folding and décollement folding may generally be oversimplified, and cannot fully account for the evolution of natural thrust-related fold systems. The recognition of the possibility that fault-related fold mechanisms can change through time may permit a better understanding of the progressive evolution of thrust-related folds.

The good agreement between our models and results from fieldwork, theoretical analyses and laboratory experiments, strongly support the applicability of sandbox modelling to study the evolution of brittle contractional structures given the limitation that the experimental multilayers are at best only a very simplified analogue of natural rocks.

Acknowledgements—We gratefully acknowledge J. Dixon, E. Erslev, and S. Marshak for their critical reviews and helpful suggestions. We wish to thank J. V. A. Keller for help during laboratory work and C. Guidi for drawing some of the figures. Howard Moore and Brian Adams are thanked for technical assistance. This research was supported by the Fault Dynamics Project (sponsored by Arco British Limited, Brasoil, U.K. Limited, BP Exploration, Conoco (U.K.) Limited, Mobil North Sea Limited, and Sun Oil Britain) and by the Italian M. U. R. S. T. (grants to F. Salvini), and CROP 11 (Director Professor M. Parotto). Fault Dynamics Publication No. 62.

REFERENCES

Alonso, J. L. and Teixell, A. (1992) Forelimb deformation in some natural examples of fault-propagation folds. In *Thrust Tectonics*, ed. K. R. McClay, pp. 175–180. Chapman and Hall, London.

Barnichon, J. D. and Charlier, R. (1996) Finite element modelling of the competition between shear bands in the early stages of thrusting: Strain localization analysis and constitutive law influence. In *Modern Developments in Structural Interpretation, Validation and Modelling*, eds P. G. Buchanan and D. A. Nieuwland, pp. 235–250. Geological Society of London Special Publication **99.**

Biot, M. A. (1961) Theory of folding of stratified visco–elastic media and its implication in tectonics and orogenesis. *Bulletin of the Geological Society, America* **72**, 1595–1632.

Bowler, S. (1987) Duplex geometry: an example from the Moine Thrust Belt. *Tectonophysics* **135**, 25–35.

Braun, J. and Sambridge, M. (1994) Dynamical Lagrangian remeshing (DLR): a new algorithm for solving large strain deformation problems and its application to fault-propagation folding. *Earth and Planetary Science Letters* **124**, 211–220.

Brown, S. P. and Spang, J. H. (1978) Geometry and mechanical relationship of folds to thrust fault propagation using a minor thrust in the Front Ranges of the Canadian Rocky Mountains. *Bulletin of Canadian Petroleum Geology* **26**, 551–571.

Butler, R. W. H. (1992) Evolution of alpine fold-thrust complexes: a linked kinematic approach. In *Structural Geology of Fold and Thrust Belts*, eds S. Mitra and G. W. Fisher, pp. 29–44. Johns Hopkins University Press, Baltimore.

Butler, R. W. H. and Bowler, S. (1995) Local displacement rate cycles in the life of a fold-thrust belt. *Terra Nova* **7**, 408–416.

Calassou, S., Laroque, C. and Malavieille, J. (1993) Transfer zones of deformation in thrust wedges: an experimental study. *Tectonophysics* **221**, 325–344.

Chester, J. S. and Chester, F. M. (1990) Fault-propagation folds above thrusts with constant dip. *Journal of Structural Geology* **7**, 903–910.

Chester, J. S., Logan, J. M. and Spang, J. H. (1991) Influence of layering and boundary conditions on fault-bend and fault-propagation folding. *Bulletin of the Geological Society, America* **103**, 1059–1072.

Cobbold, P. R., Cosgrove, J. W. and Summers, J. M. (1971) Development of internal structures in deformed anisotropic rocks. *Tectonophysics* **12**, 23–53.

Couples, G. D., Stearn, D. L. and Handin, J. W. (1994) Kinematics of experimental forced folds and their relevance to cross-section balancing. *Tectonophysics* **233**, 193–213.

Couzens, B. A. and Dunne, W. M. (1994) Displacement transfer at thrust terminations: the Saltville thrust and Sinking Creek anticline, Virginia, U.S.A. *Journal of Structural Geology* **16**, 781–793.

Dahlstrom, C. D. A. (1969) Balanced cross-sections. *Canadian Journal of Earth Science* **6**, 743–757.

Dahlstrom, C. D. A. (1970) Structural geology of the eastern margin of the Canadian Rocky Mountains. *Bulletin of Canadian Petroleum Geology* **18**, 332–406.

Davis, D., Suppe, J. and Dahlen, F. A. (1983) Mechanics of fold and thrust belts and accretionary wedges. *Journal of Geophysical Research* **88**, 1153–1172.

Dennis, J. (1972) *Structural Geology*. John Wiley, New York.

Dixon, J. M. and Liu, S. (1992) Centrifuge modelling of the propagation of thrust faults. In *Thrust Tectonics*, ed. K. R. McClay, pp. 53–69. Chapman and Hall, London.

Eisenstadt, G. and De Paor, D. G. (1987) Alternative model of thrust fault propagation. *Geology* **15**, 630–633.

Ellis, M. A. and Dunlap, W. J. (1988) Displacement variation along thrust faults: implications for the development of large faults. *Journal of Structural Geology* **10**, 183–192.

Epard, J. L. and Groshong, R. H. (1995) Kinematic model of detachment folding including limb rotation, fixed hinges and layer-parallel strain. *Tectonophysics* **247**, 85–103.

Erickson, S. G. and Jamison, W. R. (1995) Viscous–plastic finite-element models of fault-bend folds. *Journal of Structural Geology* **17**, 561–573.

Erslev, E. A. (1991) Trishear fault-propagation folding. *Geology* **19**, 617–620.

Faill, R. T. (1973) Kink band folding, Valley and Ridge province, Pennsylvania. *Bulletin of the Geological Society, America* **84**, 1289–1314.

Fisher, D. M. and Anastasio, D. J. (1994) Kinematic analysis of a large-scale leading edge fold, Lost River Range, Idaho. *Journal of Structural Geology* **16**, 337–354.

Fisher, M. P., Woodward, N. B. and Mitchell, M. M. (1992) The kinematics of break-thrust folds. *Journal of Structural Geology* **14**, 451–460.

Fowler, T. J. and Winsor, C. N. (1996) Evolution of chevron folds by profile shape changes: comparison between multilayer deformation experiments and folds of the Bendigo–Castlemaine goldfields, Australia. *Tectonophysics* **258**, 125–150.

Fox, F. G. (1959) Structure and accumulation of hydrocarbons in southern Foothills, Alberta, Canada. *Bulletin of the American Association of Petroleum Geologists* **43**, 992–1025.

Friedman, M., Hugman, R. H. H. and Handin, J. (1980) Experimental folding of rocks under confining pressure, Part VIII — Forced folding of unconsolidated sand and of lubricated layers of limestone and sandstone. *Bulletin of the Geological Society, America* **91**, 307–312.

Geiser, P. A. (1988) Mechanisms of thrust propagation: some examples and implications for the analysis of overthrust terranes. *Journal of Structural Geology* **10**, 829–845.

Goff, D. F. and Wiltschko, D. V. (1992) Stresses beneath a ramping thrust sheet. *Journal of Structural Geology* **14**, 437–449.

Goff, D. F., Wiltschko, D. V. and Fletcher, R. C. (1996) Décollement folding as a mechanism for thrust-ramp spacing. *Journal of Geophysical Research* **101**, 11341–11352.

Gretener, P. E. (1972) Thoughts on overthrust faulting in a layered sequence. *Bulletin of Canadian Petroleum Geology* **20**, 583–607.

Griffith, A. A. (1924) Theory of rupture. In *Proceedings of the First International Congress Applied Mechanics, Delft*, pp. 55–63.

Gutscher, M. A., Kukowski, N., Malavieille, J. and Lallemand, S. (1996) Cyclical behavior of thrust wedges: Insights from high basal friction sandbox experiments. *Geology* **24**, 135–138.

Hathaway, T. M. and Gayer, R. A. (1995) 3-D geometry and displacement variation of thrust faults. *Terra abstracts* (supplement to *Terra nova* **7**), 273.

Hedlund, C. A., Anastasio, D. J. and Fisher, D. M. (1994) Kinematics of fault-related folding in a duplex, Lost River Range, Idaho, U.S.A. *Journal of Structural Geology* **16**, 571–584.

Heim, A. (1919) *Geologie der Schweiz*. Touchnitz, Leipzig.

Homza, T. X. and Wallace, W. K. (1995) Geometric and kinematic models for detachment folds with fixed and variable detachment depths. *Journal of Structural Geology* **17**, 575–588.

Jamison, W. R. (1987) Geometric analysis of fold development in overthrust terranes. *Journal of Structural Geology* **9**, 207–219.

Jamison, W. R. and Pope, A. (1996) Geometry and evolution of a fault-bend fold: Mount Bertha anticline. *Bulletin of the Geological Society, America* **108**, 208–224.

Johnson, A. M. (1995) Orientations of faults determined by premonitory shear zones. *Tectonophysics* **247**, 161–238.

Kilsdonk, B. and Wiltschko, D. V. (1988) Deformation mechanisms in the southeastern ramp region of the Pine Mountain block Tennessee. *Bulletin of the Geological Society, America* **100**, 653–664.

Koyi, H. (1995) Mode of internal deformation in sand wedges. *Journal of Structural Geology* **17**, 293–300.

Lallemand, S. E., Malavieille, J. and Calassou, S. (1992) Effects of oceanic ridge subduction on accretionary wedges: Experimental modeling and marine observations. *Tectonics* **11**, 1301–1313.

Lan, L. and Hudleston, P. J. (1995) The effects of rheology on the strain distribution in single layer buckle folds. *Journal of Structural Geology* **17**, 727–738.

Liu, S. and Dixon, J. M. (1990) Centrifuge modelling of thrust faulting: strain partitioning and sequence of thrusting in duplex structures. In *Deformation Mechanisms, Rheology and Tectonics*, ed. R. J. Knipe, pp. 431–434. Geological Society of London Special Publication **54**.

Liu, S. and Dixon, J. M. (1991) Centrifuge modelling of thrust faulting: structural variations along strike in fold-thrust belts. *Tectonophysics* **188**, 39–62.

Liu, S. and Dixon, J. M. (1995) Localization of duplex thrust-ramps by buckling: analog and numerical modelling. *Journal of Structural Geology* **17**, 875–886.

Liu, H., McClay, K. R. and Powell, D. (1992) Physical models of thrust wedges. In *Thrust Tectonics*, ed. K. R. McClay, pp. 71–81. Chapman and Hall, London.

Malavieille, J. (1984) Modélisation expérimentale des chevauchements imbriqués: Application aux chaînes de montagnes. *Bulletin of the Geological Society, France* **7**, 129–138.

Mandl, G. (1988) *Mechanics of Tectonic Faulting. Models and Basic Concepts*. Elsevier, Amsterdam.

Markley, M. and Wojtal, S. (1996) Mesoscopic structure, strain, and volume loss in folded cover strata, Valley and Ridge Province, Maryland. *American Journal of Science* **296**, 23–57.

Marshak, S. and Wilkerson, M. S. (1992) Effect of overburden thickness on thrust belt geometry and development. *Tectonics* **11**, 560–566.

McClay, K. R. (1990a) Deformation mechanics in analogue models of extensional fault systems. In *Deformation Mechanisms, Rheology and Tectonics*, eds R. J. Knipe and E. H. Rutter, pp. 445–453. Geological Society of London, Special Publication **54.**

McClay, K. R. (1990b) Extensional fault systems in sedimentary basins. A review of analogue model studies. *Marine and Petroleum Geology* **7**, 206–233.

McNaught, M. A. and Mitra, G. (1993) A kinematic model for the origin of footwall synclines. *Journal of Structural Geology* **15**, 805–808.

Medwedeff, D. A. (1989) Growth fault-bend-folding at southeast Lost Hills, San Joaquin Valley, California. *Bulletin of the American Association of Petroleum Geologists* **73**, 54–67.

Mitra, S. (1990) Fault-propagation folds: geometry, kinematic evolution, and hydrocarbon traps. *Bulletin of the American Association of Petroleum Geologists* **74**, 921–945.

Mitra, S. (1992) Balanced structural interpretations in fold and thrust belts. In *Structural Geology of Fold and Thrust Belts*, eds S. Mitra and G. W. Fisher, pp. 53–77. John Hopkins University Press.

Mitra, S. (1993) Geometry and kinematic evolution of inversion structures. *Bulletin of the American Association of Petroleum Geologists* **77**, 1159–1191.

Morgan, J. K. and Karig, D. E. (1995) Kinematics and a balanced and restored cross-section across the toe of the eastern Nankai accretionary prism. *Journal of Structural Geology* **17**, 31–45.

Morley, C. K. (1994) Fold-generated imbricates: examples from the Caledonides of Southern Norway. *Journal of Structural Geology* **16**, 619–631.

Mulugeta, G. (1988) Modelling the geometry of Coulomb thrust wedges. *Journal of Structural Geology* **10**, 847–859.

Mulugeta, G. and Koyi, H. (1992) Episodic accretion and strain partitioning in a model sand wedge. *Tectonophysics* **202**, 319–333.

Narr, W. and Suppe, J. (1994) Kinematics of basement-involved compressive structures. *American Journal of Science* **294**, 802–860.

Ramberg, H. (1981) *Gravity, Deformation and the Earth's Crust*. Academic Press, New York.

Rich, J. L. (1934) Mechanics of low angle overthrust faulting as illustrated by Cumberland thrust block, Virginia, Kentuchy and Tennessee. *Bulletin of the American Association of Petroleum Geologists* **18**, 1584–1596.

Royse, F., Jr, Warner, M. A. and Reese, D. L. (1975) Thrust belt structural geometry and related stratigraphic problems—Wyoming, Idaho, northern Utah. *Rocky Mountain Association of Geologists, Symposium on Deep Drilling Frontier in Central Rocky Mountains*, 41–54.

Sherwin, J. and Chapple, W. M. (1968) Wavelengths of single layer folds: a comparison between theory and observations. *American Journal of Science* **266**, 167–179.

Stewart, K. G. and Alvarez, W. (1991) Mobile-hinge kinking in layered rocks and models. *Journal of Structural Geology* **13**, 243–259.

Storti, F. and McClay, K. (1995) The influence of sedimentation on the growth of thrust wedges in analogue models. *Geology* **23**, 999–1002.

Storti, F. and Poblet, J. (1994) *The Role of Growth Strata to Infer the Kinematics of Shallow Foreland Thrust Tip Folds*. Fault Dynamics workshop, Royal Holloway University of London, Egham, March, 28–30 (1994), abstract volume, 42.

Storti, F. and Salvini, F. (1996) Progressive rollover fault-propagation folding: a possible kinematic mechanism to generate regional scale recumbent folds in shallow foreland belts. *Bulletin of the American Association of Petroleum Geologists* **80**, 174–193.

Suppe, J. (1983) Geometry and kinematics of fault-bend folding. *American Journal of Science* **283**, 684–721.

Suppe, J. and Medwedeff, D. A. (1984) Fault-propagation folding. *Bulletin of the Geological Society, America Abstracts with Programs* **16**, 670.

Suppe, J. and Medwedeff, D. A. (1990) Geometry and kinematics of fault-propagation folding. *Eclogae geologicae Helvetiae* **83**, 909–954.

Tavarnelli, E. (1994) Evidences for fault-propagation folding in the Umbria–Marche–Sabina Apennines (Central Italy). *Annales Tectonicae* **7**, 87–99.

Turcotte, D. L. and Schubert, G. (1982) *Geodynamics — Applications of Continuum Physics to Geological Problems*. John Wiley and Sons, New York, USA.

Verschuren, M., Nieuwland, D. and Gast, J. (1996) Multiple detachment levels in thrust tectonics: sandbox experiments and palinspastic reconstruction. In *Modern Developments in Structural Interpretation, Validation and Modelling*, eds P. G. Buchanan and D. A. Nieuwland, pp. 227–234. Geological Society of London, Special Publication **99**.

Wickham, J. (1995) Fault displacement–gradient folds and the structure at Lost Hills, California (U.S.A.). *Journal of Structural Geology* **17**, 1293–1302.

Williams, J. R. (1980) Similar and chevron folds in multilayers using finite elements and geometric models. *Tectonophysics* **65**, 323–338.

Williams, G. and Chapman, T. (1983) Strains developed in the hanging-walls of thrusts due to their slip/propagation rate: a dislocation model. *Journal of Structural Geology* **5**, 563–571.

Willis, B. (1893) The mechanics of Appalachian Structure. *Annual Report of the U.S. Geological Survey* **13(II)**, 211–282.

Wiltschko, D. V. and Eastman, D. (1983) Role of basement ramps in localizing thrust fault ramps. In *Contributions to the Tectonics and Geophysics of Mountain Chains*, eds R. D. Hetcher, H. Williams and I. Zietz, pp. 177–190. Geological Society of America, Memoir **158**.

Wiltschko, D. V., Medwedeff, D. A. and Millson, H. E. (1985) Distribution and mechanisms of strain within rocks on the northwest ramp of Pine Mountain Block, southern Appalachian foreland: a field test of theory. *Bulletin of the Geological Society, America* **96**, 426–435.

Woodward, N. B. (1992) Deformation styles and geometric evolution of some Idaho–Wyoming Thrust Belt structures. In *Structural Geology of Fold and Thrust Belts*, eds S. Mitra and G. W. Fisher, pp. 191–206. Johns Hopkins University Press.

Yang, X. and Gray, D. R. (1994) Strain, cleavage and microstructure variation in sandstone: implications for stiff layer behaviour in chevron folding. *Journal of Structural Geology* **16**, 1353–1365.

Zhang, Y., Hobbs, B. E., Ord, A. and Mühlhaus, H. B. (1996) Computer simulation of single-layer buckling. *Journal of Structural Geology* **18**, 643–655.